© S. Hirzel Verlag
Stuttgart

Rigorous Computation of Plate-Wave Intensity

W. Maysenhölder
Fraunhofer-Institut für Bauphysik, Stuttgart

Dedicated to Professor Dr. Fridolin P. Mechel on the occasion of his 60th birthday

Rigorous Computation of Plate-Wave Intensity

Summary

Exact analytical expressions exist for the displacement fields of elastic waves in homogeneous, isotropic, infinite plates of constant thickness. From these expressions the intensity and the time-averaged energy density of an arbitrary propagating mode at arbitrary frequency is derived without any approximation as a function of the spatial coordinate from surface to surface. Spatial averaging of these quantities across the thickness of the plate is also performed analytically and exactly. Practical application of the results to a particular mode requires the knowledge of its phase and group velocity, which in general have to be computed by numerical methods. Numerous diagrams illustrate the behaviour of the analytical expressions, especially for the quasi-longitudinal mode and the bending mode. Comparison of the exact intensity of the bending mode with the approximate expression from simple bending wave theory leads to a precise determination of the error which enters the conventional method of measuring the bending wave intensity. This offers the possibility of extending the conventional measuring technique beyond the validity of thin plate theory.

Strenge Berechnung der Intensität von Plattenwellen

Zusammenfassung

Für die Verschiebungsfelder von elastischen Wellen in homogenen, isotropen, unendlichen Platten konstanter Dicke existieren exakte analytische Ausdrücke. Daraus werden die Intensität und die zeitlich gemittelte Energiedichte einer beliebigen ausbreitungsfähigen Mode bei beliebiger Frequenz als Funktion der räumlichen Koordinate von Oberfläche zu Oberfläche ohne jegliche Näherung abgeleitet. Die räumliche Mittelung dieser Größen über die Plattendicke wird ebenfalls analytisch und exakt ausgeführt. Die praktische Anwendung der Ergebnisse auf eine bestimmte Mode erfordert die Kenntnis ihrer Phasen- und Gruppengeschwindigkeit, welche im allgemeinen mit numerischen Methoden berechnet werden müssen. Zahlreiche Diagramme veranschaulichen das Verhalten der analytischen Ausdrücke, insbesondere für die quasilongitudinale Mode und die Biegemode. Ein Vergleich der exakten Intensität der Biegemode mit der Näherung aus der einfachen Biegewellentheorie führt zu einer genauen Bestimmung des Fehlers, der in das konventionelle Meßverfahren für Biegewellenintensitäten eingeht. Damit besteht die Möglichkeit, das konventionelle Meßverfahren über den Gültigkeitsbereich der einfachen Biegewellentheorie hinaus anzuwenden.

Le calcul rigoureux de l'intensité des ondes dans une plaque

Sommaire

Il existe des expressions analytiques exactes pour les champs du déplacement des ondes élastiques dans des plaques homogènes, isotropes, infinies et d'épaisseur constante. A partir de ces expressions, on a pu déduire, sans approximation aucune, les intensités et les moyennes temporelles de la densité d'énergie à une fréquence quelconque et pour un mode arbitraire, pourvu qu'il soit capable de se propager, en fonction de la coordonnée d'espace mesurée de surface à surface. La moyenne spatiale de ces quantités à travers l'épaisseur de la plaque se fait également par voie analytique et sans approximation. L'application pratique de ces résultats à un mode particulier exige en fait la connaissance de ses vitesses de phase et de groupe, données qui ne sont en général accessibles qu'à des méthodes numériques. De nombreux diagrammes illustrent le comportement des expressions analytiques, spécialement pour le mode quasi-longitudinal et le mode de flexion. Une comparaison entre l'intensité exacte du mode de flexion et son approximation provenant de la théorie simplifiée des ondes de flexion permet une détermination précise de l'erreur qui entache la méthode traditionnelle de mesure de l'intensité de ces ondes. Ainsi apparaît la possibilité d'une extension de la technique classique de ce type de mesures au delà même de la validité de la théorie des plaques minces.

1. Introduction

Measuring the intensity of bending waves in (homogeneous and isotropic) plates and beams has become quite popular and above all very useful for a variety of applications. It has been introduced by Noiseux twenty years ago [1] and was further developed and applied by numerous authors (see e.g. [2–10]). All of this work is based on simple bending wave theory, which is valid for thin plates (or beams), i.e. in the low-frequency limit. Fortunately, this approximation is sufficient for many applications. Sometimes, however, one would like to know how serious the error is, if in such a

Received 30 April 1990,
accepted 4 May 1990.

Dr. rer. nat. W. Maysenhölder, Fraunhofer-Institut für Bauphysik, Nobelstr. 12, 7000 Stuttgart 80.

measurement the frequency is raised beyond the range of thin plate theory. It may be readily assumed that the measured intensity direction is still correct [10], but what about the magnitude?

Apparently there are only very few places in the literature where the intensity of plate waves is evaluated for higher frequencies. Explicit expressions for energy density and intensity of pure shear modes (SH-waves) can be found in the textbook by Achenbach [11]. Analytical results for Rayleigh-waves are also available, but probably not well-known [12–14]. To the author's knowledge the case of non-pure-shear-modes at intermediate frequencies has been treated so far only once, viz. by Tamm and Weis [15], who present some numerical results in the form of diagrams.

It is the main purpose of the present paper to communicate analytical expressions for the energy density and intensity of plate waves at arbitrary frequency. No approximations are involved. The only prerequisite for the application of the expressions to a particular mode is the knowledge of its phase and group velocity. In general, these have to be obtained numerically, but they can be calculated with any desired accuracy. Numerous diagrams visualize the results for a typical Poisson's ratio $\sigma = 0.3$.

2. Fundamental equations

We consider an infinite plate of thickness h consisting of a material which is homogeneous and isotropic, and which is characterized by Lamé's constants λ and μ or by Young's modulus E and Poisson's ratio σ, and by its mass density ϱ. All waves are assumed straight-crested and propagating along the x-direction (Fig. 1). Then the displacement vector $\boldsymbol{u}$ of a particular mode can be written in the form

$$\boldsymbol{u}(r,t) = \begin{pmatrix} u_x(y) \\ u_y(y) \\ u_z(y) \end{pmatrix} e^{i(kx-\omega t)}. \tag{1}$$

Only real k and real ω are considered in this paper.

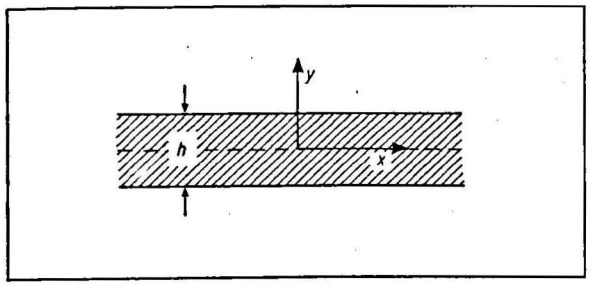

Fig. 1. Coordinates describing a plate of thickness h. The z-direction is perpendicular to the drawing plane.

Plate modes are classified into four families [16]. The first two families show displacements along the z-direction only ($u_x = u_y = 0$), while the last two families possess no z-component ($u_z = 0$). The subdivision in each group of families is by symmetry.

In the following the form of the displacement field of each family of modes is given together with the dispersion relation, from which phase velocity $c = \omega/k$ and group velocity $C = \mathrm{d}\omega/\mathrm{d}k$ can be calculated.

The first two families contain only pure shear modes with symmetric displacements

$$u_z = A\cos(n\pi y/h), \quad n = 0, 2, 4, \ldots \tag{2}$$

or with antisymmetric displacements

$$u_z = A\sin(n\pi y/h), \quad n = 1, 3, 5, \ldots \tag{3}$$

(A denotes arbitrary amplitudes). Both families together are sometimes called SH-waves (a term from seismology: Shear-Horizontal). In fact, they can often by described by the same formula, e.g. in the case of the phase velocity c,

$$c^2 = c_t^2\left[1 + \left(\frac{n\pi}{kh}\right)^2\right] = \frac{c_t^2}{\left[1 - \left(\frac{nc_t}{2fh}\right)^2\right]}, \tag{4}$$

where even n refers to the symmetric family and odd n to the antisymmetric one (c_t = velocity of transversal waves in a three-dimensionally infinite medium, $f = \omega/2\pi$). The group velocity C is reciprocal to the phase velocity for a particular value of n:

$$Cc = c_t^2. \tag{5}$$

The remaining two families of plate modes are usually much more important in practice but – as is well-known – unfortunately also much more complicated. The displacement field of the symmetric family reads

$$\begin{aligned} u_x &= \mathrm{i}A\ [\cosh(\alpha_1 k y) - \alpha_x R_s \cosh(\alpha_2 k y)], \\ u_y &= \alpha_1 A[\sinh(\alpha_1 k y) - \alpha_y R_s \sinh(\alpha_2 k y)], \end{aligned} \tag{6}$$

and that of the antisymmetric one is obtained by exchanging sinh and cosh:

$$\begin{aligned} u_x &= \mathrm{i}A\ [\sinh(\alpha_1 k y) - \alpha_x R_a \sinh(\alpha_2 k y)], \\ u_y &= \alpha_1 A[\cosh(\alpha_1 k y) - \alpha_y R_a \cosh(\alpha_2 k y)]. \end{aligned} \tag{7}$$

The new symbols are defined as follows:

$$\begin{aligned} \alpha_1 &= \sqrt{1-(c/c_t)^2}, & \alpha_2 &= \sqrt{1-(c/c_t)^2}, \\ \alpha_x &= \frac{2\alpha_1\alpha_2}{1+\alpha_2^2}, & \alpha_y &= \frac{2}{1+\alpha_2^2}, \\ R_s &= \frac{\sinh(\alpha_1 k h/2)}{\sinh(\alpha_2 k h/2)}, & R_a &= \frac{\cosh(\alpha_1 k h/2)}{\cosh(\alpha_2 k h/2)}, \end{aligned} \tag{8}$$

with the velocity c_l of longitudinal waves in a three-dimensionally infinite medium. Both families possess one symmetric and one antisymmetric displacement component with respect to a sign change of the coordinate y. Why then should one family be called symmetric and the other one antisymmetric? What is meant is the behaviour of the displacement vector upon reflexion by a mirror plane $y = 0$ rather than upon reflexion with respect to a point. This operation changes the sign of the y-component, but not the signs of the x- and z-components. In the case of the symmetric modes (6) the displacements for $y < 0$ can be obtained from the corresponding ones with $y > 0$ by just this reflexion at the plane $y = 0$, while for the antisymmetric modes (7) an additional sign change is necessary.

The phase velocities have to be computed from the Rayleigh-Lamb frequency equations

$$\frac{4\alpha_1\alpha_2}{(1+\alpha_2^2)^2} = \left[\frac{\tanh(\alpha_2 k h/2)}{\tanh(\alpha_1 k h/2)}\right]^{\pm 1}, \tag{9}$$

where the plus sign applies to the symmetric family and the minus sign to the antisymmetric family of modes with vanishing z-component. (Some details of the numerical treatment of (9) are given in the appendix.) The fundamental mode of each family, i.e. the mode with the lowest phase velocity, is of particular importance and often named after its low-frequency behaviour as quasi-longitudinal mode and bending (flexural) mode, respectively. In the high-frequency limit both fundamental modes become Rayleigh surface waves.

Having introduced the basic nomenclature we now can address the actual subject of the present paper: Energy and energy transport of plate waves. Energy density $e(\boldsymbol{r}, t)$ and energy flux $\boldsymbol{S}(\boldsymbol{r}, t)$ are given as a function of position $\boldsymbol{r}$ and time t by

$$e = \tfrac{1}{2}(\varrho\, \boldsymbol{v}\cdot\boldsymbol{v} + \underline{\sigma} \cdot\cdot\, \underline{\varepsilon}), \tag{10}$$

$$\boldsymbol{S} = -\,\underline{\sigma}\cdot\boldsymbol{v} \tag{11}$$

with particle velocity $\boldsymbol{v}$, stress tensor $\underline{\sigma}$ and strain tensor $\underline{\varepsilon}$. All quantities in eqs. (10) and (11) are assumed to be real, i.e. evaluation from the displacement fields (1) implies taking the real (or imaginary) part only. This is a somewhat cumbersome procedure. In order to benefit from the complex notation of (1) we will confine ourselves to temporal averages. Thus we obtain for the temporal average $w_{kin}(\boldsymbol{r})$ of the kinetic energy density

$$w_{kin} = \frac{\varrho}{4}\mathrm{Re}\{\boldsymbol{v}\cdot\boldsymbol{v}^*\}, \tag{12}$$

for the temporal average $w_{pot}(\boldsymbol{r})$ of the potential energy density

$$w_{pot} = \tfrac{1}{4}\mathrm{Re}\{\underline{\sigma} \cdot\cdot\, \underline{\varepsilon}^*\}, \tag{13}$$

and for the temporal average of the energy flux, the intensity $\boldsymbol{I}(\boldsymbol{r})$,

$$\boldsymbol{I} = -\tfrac{1}{2}\mathrm{Re}\{\underline{\sigma}\cdot\boldsymbol{v}^*\}. \tag{14}$$

Additional spatial averaging reduces to averaging across the plate's thickness, because the temporal averages are independent of x and z:

$$\langle w_{kin}\rangle = \frac{1}{h}\int_{-h/2}^{+h/2} w_{kin}(y)\,\mathrm{d}y. \tag{15}$$

This integration will be performed analytically for all plate modes in the following sections. In principle this could be done as well for the remaining space-time averages $\langle w_{pot}\rangle$ and $\langle I\rangle$. This, however, would be quite awkward and it can be avoided if one takes advantage of two theorems.

The first one states that the space-time averages of kinetic and potential energy densities for a particular mode are equal:

$$\langle w_{kin}\rangle = \langle w_{pot}\rangle. \tag{16}$$

This relation is usually taken for granted and not explicitly mentioned. It can be proved under rather general conditions on the basis of the virial theorem. (This proof will be published elsewhere [17]. It is surprising that it could not be found in the literature.)

The second theorem relates intensity, total energy density $w = w_{kin} + w_{pot}$ and group velocity and was proved by Biot [18]. We formulate it for the x-component of the intensity because the other components are zero (see following sections):

$$\langle I_x\rangle = C\langle w\rangle. \tag{17}$$

By means of eqs. (16) and (17) the space-time average of the intensity of a plate wave can be determined very easily from $\langle w_{kin}\rangle$.

3. Normalization

Normalization of quantities is a useful method of reducing the number of independent variables. Unfortunately, it can be done in different ways and therefore normalized results may not always be comparable with each other without some conversion. We follow the usual practice and measure all velocities in units of c_t, the phase velocity of the fundamental symmetric shear mode, which is the only non-dispersive plate mode. For the frequency $f = \omega/2\pi$ we adopt the normalization of Cremer and Heckl [19] by c_t/h. As a

consequence the length unit is equal to the plate's thickness h.

We are free to choose a third unit for material properties and select the modulus $\lambda + 2\mu$ related to longitudinal waves in an infinite solid. This selection has the advantage of involving both Lamé's constants, i.e. both shear and compressional modulus, and is always positive. The units of other quantities are now fixed, e.g. $(\lambda + 2\mu)/c_t^2$ for mass density, $(\lambda + 2\mu)h^3$ for energy, $\lambda + 2\mu$ for energy density, and $(\lambda + 2\mu)c_t$ for energy flux and intensity. For an iron plate with $\sigma = 0.3$, $E = 200$ GPa, $\varrho = 7800$ kg m^{-3}, $h = 0.01$ m these units amount to the following values:

$$\begin{aligned}
c_t &= 3140\ \mathrm{ms}^{-1},\\
c_t/h &= 314\ \mathrm{kHz},\\
h/c_t &= 3.18\ \mu\mathrm{s},\\
(\lambda+2\mu)/c_t^2 &= 27300\ \mathrm{kg\,m}^{-3},\\
\lambda+2\mu &= 269\ \mathrm{GPa} = 269\ \mathrm{GJ\,m}^{-3},\\
(\lambda+2\mu)h^3 &= 269\ \mathrm{kJ},\\
(\lambda+2\mu)c_t &= 845\ \mathrm{TW\,m}^{-2} = 8.45\cdot 10^{14}\ \mathrm{W\,m}^{-2}. \qquad (18)
\end{aligned}$$

At first sight the last number may appear astronomically high and not very suitable for measuring intensities of elastodynamic waves. In order, however, to get a number for the intensity of a wave, its amplitude has to be specified; and in the spirit of normalization the amplitude is set equal to the length unit, the plate's thickness, leading to unrealistically high intensities. For this reason the normalized quantities will assume values around unity, which is convenient for the diagrams. If one is to apply the results of the theory to an experimental situation, conversion to the measured quantities is necessary anyway, irrespective of the size of the normalization units.

In the following all quantities are assumed to be normalized as described above (and therefore dimensionless) without introducing new symbols. Formally this can be achieved by

$$c_t = h = \lambda + 2\mu = 1. \qquad (19)$$

Some useful relations in accordance with (19) are listed below:

$$\begin{aligned}
\lambda &= \frac{\sigma}{1-\sigma}, \quad \mu = \frac{1-2\sigma}{2-2\sigma},\\
c_l^2 &= \frac{2-2\sigma}{1-2\sigma}, \quad \mu = c_l^{-2},\\
\varrho &= \mu. \qquad (20)
\end{aligned}$$

4. Pure shear modes

Energy density and intensity of pure shear modes are easily derived from the displacements (2) and (3) and the velocity relations (4) and (5) [11]. The results are given here for completeness and for the convenience of the reader. The amplitude of each mode is chosen such that

$$u_z(y = \tfrac{1}{2}) = 1, \qquad (21)$$

i.e. $|A| = 1$ in (2) and (3). This leads to

$$w_{\mathrm{kin}}(y) = \pi^2 \mu f^2 |u_z|^2 \qquad (22)$$

where

$$|u_z|^2 = \begin{cases} \cos^2(n\pi y) & \text{for } n \text{ even} \\ \sin^2(n\pi y) & \text{for } n \text{ odd}. \end{cases} \qquad (23)$$

With the strain tensor

$$\underline{\varepsilon} = \frac{1}{2}\begin{pmatrix} 0 & 0 & \mathrm{i}ku_z \\ 0 & 0 & u_z' \\ \mathrm{i}ku_z & u_z' & 0 \end{pmatrix} \mathrm{e}^{\mathrm{i}(kx-\omega t)} \qquad (24)$$

and the stress tensor $\underline{\sigma} = 2\mu\,\underline{\varepsilon}$ one obtains

$$w_{\mathrm{pot}}(y) = \tfrac{1}{4}\mu[k^2|u_z|^2 + |u_z'|^2], \qquad (25)$$

where a prime indicates differentiation with respect to y:

$$|u_z'|^2 = \begin{cases} n^2\pi^2 \sin^2(n\pi y) & \text{for } n \text{ even} \\ n^2\pi^2 \cos^2(n\pi y) & \text{for } n \text{ odd}. \end{cases} \qquad (26)$$

At the frequency $f = n/\sqrt{2}$ w_{pot} is constant over the cross-section of the plate.

Locally, w_{kin} and w_{pot} are different in general (except for $n = 0$ where they are the same everywhere), however, upon averaging one recovers equality (16)

$$\langle w_{\mathrm{kin}} \rangle = \langle w_{\mathrm{pot}} \rangle = \frac{\pi^2}{2}\mu f^2. \qquad (27)$$

The space-time average of the energy density is the same for all pure shear modes provided the amplitude at the plate surface is of equal magnitude! By contrast the averaged intensity

$$\langle I_x \rangle = \pi^2 \mu C f^2 = \pi^2 \mu \sqrt{1 - \frac{n^2}{4f^2}}\, f^2 \qquad (28)$$

depends on n, because the group velocity C is different for different modes. Theorem (17) can be directly proven by integrating the expression

$$I_x(y) = 2\pi^2 \mu |u_z|^2 \sqrt{1 - \frac{n^2}{4f^2}}\, f^2 \qquad (29)$$

which has been evaluated from (14). As expected, only the shear modulus μ enters the expressions.

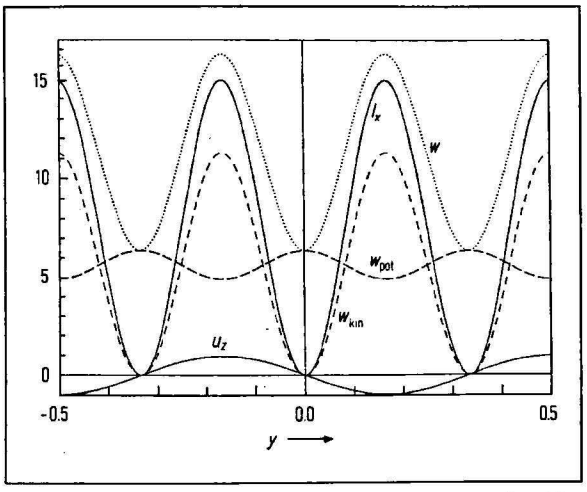

Fig. 2. Displacement component $u_z(y)$, energy densities $w_{kin}(y) + w_{pot}(y) = w(y)$, and intensity $I_x(y)$ of the shear mode $n = 3$ at the frequency $f = 2$ ($\sigma = 0.3$).

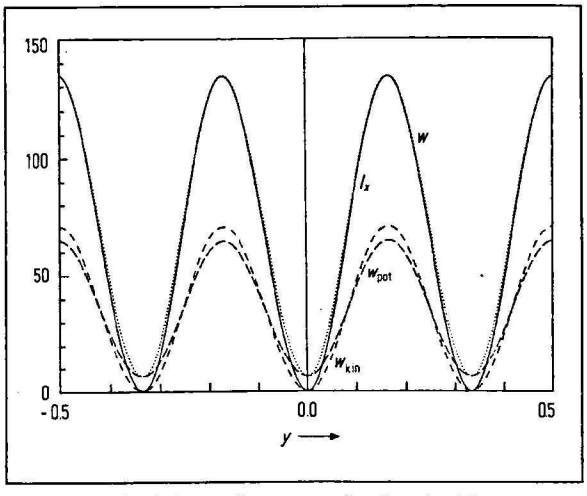

Fig. 3. As Fig. 2, but a frequency $f = 5$ and without u_z.

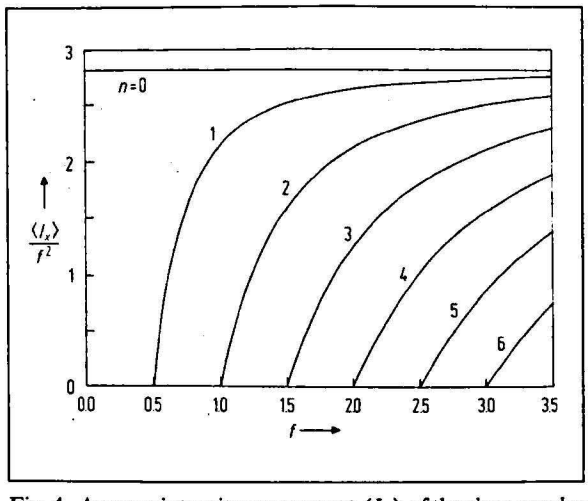

Fig. 4. Average intensity component $\langle I_x \rangle$ of the shear modes $n = 0 \ldots 6$ divided by the frequency squared versus frequency ($\sigma = 0.3$).

In order to provide a non-trivial illustration, the shear mode $n = 3$ at the frequency $f = 2$ (which is close to the cut-on frequency 1.5) has been selected for Fig. 2.

With increasing frequency w_{pot} approaches w_{kin}, the group velocity approaches one, and thus I_x approaches w (Fig. 3). In the limit of infinite frequency the average intensities of all modes become equal:

$$\langle I_x \rangle = \pi^2 \mu f^2 \tag{30}$$

(see Fig. 4).

5. Non-pure-shear modes

This section contains the general relations for all the modes with vanishing u_z-component. The time-averaged kinetic energy density is simply

$$w_{kin}(y) = \pi^2 \mu f^2 [|u_x|^2 + |u_y|^2]. \tag{31}$$

For the potential part the strain tensor

$$\underline{\varepsilon} = \frac{1}{2} \begin{pmatrix} 2ik u_x & u_x' + ik u_y & 0 \\ u_x' + ik u_y & 2u_y' & 0 \\ 0 & 0 & 0 \end{pmatrix} e^{i(kx - \omega t)} \tag{32}$$

and the stress tensor

$$\underline{\sigma} = \begin{pmatrix} ik u_x + \lambda u_y' & \mu(u_x' + ik u_y) & 0 \\ \mu(u_x' + ik u_y) & u_y' + \lambda ik u_x & 0 \\ 0 & 0 & 0 \end{pmatrix} e^{i(kx - \omega t)} \tag{33}$$

combine to

$$w_{pot}(y) = \tfrac{1}{4} [k^2 |u_x|^2 + |u_y'|^2 + 2\lambda k \operatorname{Im}\{u_x^* u_y'\} + \mu |u_x' + ik u_y|^2]. \tag{34}$$

Finally, the x-component of the intensity is given by

$$I_x(y) = \pi f [(|u_x|^2 + \mu |u_y|^2) k + \lambda \operatorname{Im}\{u_x^* u_y'\} + \mu \operatorname{Im}\{u_x' u_y^*\}]. \tag{35}$$

It is evident from (33) and $u_z = 0$ that the z-component of the intensity is zero. The y-component

$$I_y(y) = \pi f [\operatorname{Re}\{u_x^* u_y\} k + \lambda \operatorname{Im}\{u_y^* u_y'\} + \mu \operatorname{Im}\{u_x^* u_x' + 2u_y^* u_y'\}] \tag{36}$$

can also be shown to vanish everywhere. It is certainly true if $u_x^* u_y$ is imaginary and $u_x^* u_x'$ and $u_y^* u_y'$ are real. A detailed discussion of the three velocity ranges $c \leqq 1$, $1 < c \leqq c_l$, $c_l < c$ reveals that each displacement component is either real or imaginary (assume a real amplitude A for simplicity) and the product of x- and y-component is always imaginary. Hence $I_y = 0$ follows immediately from (36).

As a supplement to eqs. (6) and (7) we also list the derivatives of the displacement components for symmetric modes,

$$u_x'(y) = \mathrm{i}\,k\,A\ [\alpha_1 \sinh(\alpha_1 k y) - \alpha_2 \alpha_x R_s \sinh(\alpha_2 k y)], \tag{37}$$
$$u_y'(y) = \alpha_1 k A [\alpha_1 \cosh(\alpha_1 k y) - \alpha_2 \alpha_y R_s \cosh(\alpha_2 k y)].$$

and for antisymmetric modes,

$$u_x'(y) = \mathrm{i}\,k\,A\ [\alpha_1 \cosh(\alpha_1 k y) - \alpha_2 \alpha_x R_a \cosh(\alpha_2 k y)], \tag{38}$$
$$u_y'(y) = \alpha_1 k A [\alpha_1 \sinh(\alpha_1 k y) - \alpha_2 \alpha_y R_a \sinh(\alpha_2 k y)].$$

In principle, all energy quantities could be averaged analytically over the cross-section of the plate, because only hyperbolic functions are involved. Fortunately (see section 3) it suffices to perform the integration for the simplest quantity, w_{kin}, only. We obtain for symmetric modes

$$\langle w_{kin}\rangle = \frac{\pi^2}{2}\mu f^2 |A|^2 \{(S_1+1) + |\alpha_x|^2 |R_s|^2 (S_2+1) + |\alpha_1|^2 [|S_1-1| + |\alpha_y|^2 |R_s|^2 |S_2-1|] - 4\alpha_1^2 \alpha_y S_1\}, \tag{39}$$

and for antisymmetric modes

$$\langle w_{kin}\rangle = \frac{\pi^2}{2}\mu f^2 |A|^2 \{|S_1-1| + |\alpha_x|^2 |R_a|^2 |S_2-1| + |\alpha_1|^2 [(S_1+1) + |\alpha_y|^2 |R_a|^2 (S_2+1)] - 4|\alpha_1|^2 \alpha_y S_1\}, \tag{40}$$

with

$$S_m = \frac{\sinh(\alpha_m k)}{\alpha_m k} \quad (m = 1, 2). \tag{41}$$

Note the little difference between (39) and (40) in the last term. It is essential for imaginary α_1, i.e. for $c > c_l$.

With the aid of the relations (16) and (17) the spatial average of the intensity can be calculated from (39) or (40) for any plate mode with $u_z = 0$ in a straightforward manner. No approximations have been involved in the course of the derivation of the above expressions and the accuracy of the results depends only (apart from round-off errors etc.) on the accuracy of the phase and group velocities, which are needed as inputs. The special cases of the two fundamental modes will now be discussed in detail in the following subsections.

5.1. The quasi-longitudinal mode

Phase and group velocity of the fundamental symmetric mode are shown in Fig. 5 for the case $\sigma = 0.3$. (The behaviour of all the results is very similar for other values of Poisson's ratio within the typical range between $\sigma = 0.2$ and $\sigma = 0.5$).

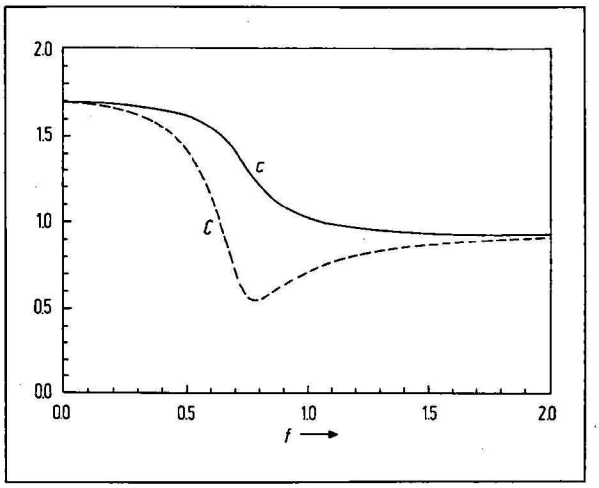

Fig. 5. Phase velocity c and group velocity C of the quasi-longitudinal mode versus frequency ($\sigma = 0.3$).

Analogous to the choice (21) for the pure shear modes the amplitude of the quasi-longitudinal mode is chosen such that the displacement component dominating at low frequencies is equal to unity at the surface $y = 1/2$:

$$u_x(y = \tfrac{1}{2}) = 1. \tag{42}$$

The displacement field varies considerably as a function of frequency (Fig. 6). While at $f = 0.5$ it looks still similar to its behaviour in the limit $f \to 0$ (constant u_x and small linear u_y), the longitudinal component u_x points in opposite directions at the surface and in the middle of the plate at intermediate frequencies. The surface-wave behaviour is exemplified at $f = 10$. At the surface the longitudinal component is dominant only at low frequencies!

The y-dependence of the various energy quantities at the four frequencies of Fig. 6 can be studied in Fig. 7. Except at low frequencies, where the variation over the cross-section is smooth and small, there is a pronounced local minimum of w_{pot} just below the surface; w and I_x reach their maximum values at the surface.

The values at the surface as a function of frequency are shown in Fig. 8. Both at low and at high frequencies these surface quantities are evidently proportional to the frequency squared. The most conspicuous feature of Fig. 8 is the singularity of w_{kin} at $f = \frac{1}{2}\sqrt{2}$, which is caused by the convention (42). At this particular frequency phase and group velocity are independent of σ(!) and known analytically:

$$c = \sqrt{2}, \quad C = \tfrac{1}{2}\sqrt{2}. \tag{43}$$

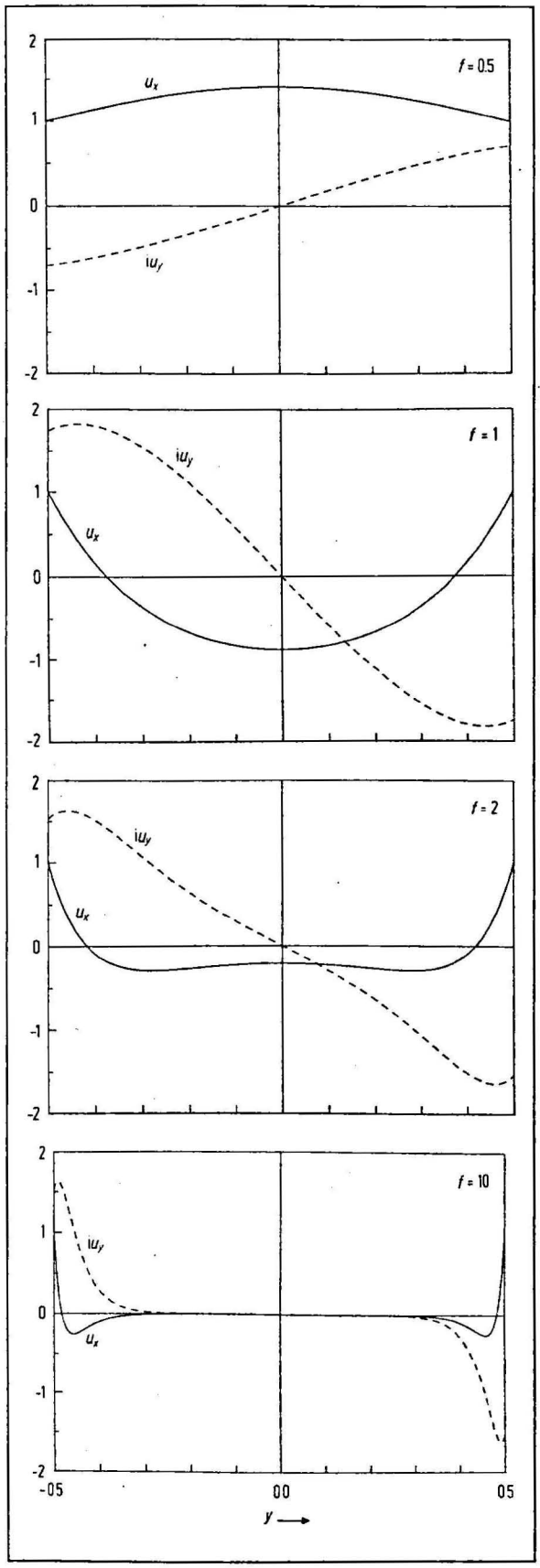

Fig. 6. Displacement components $u_x(y)$ and $u_y(y)$ of the quasi-longitudinal mode at various frequencies f ($\sigma = 0.3$).

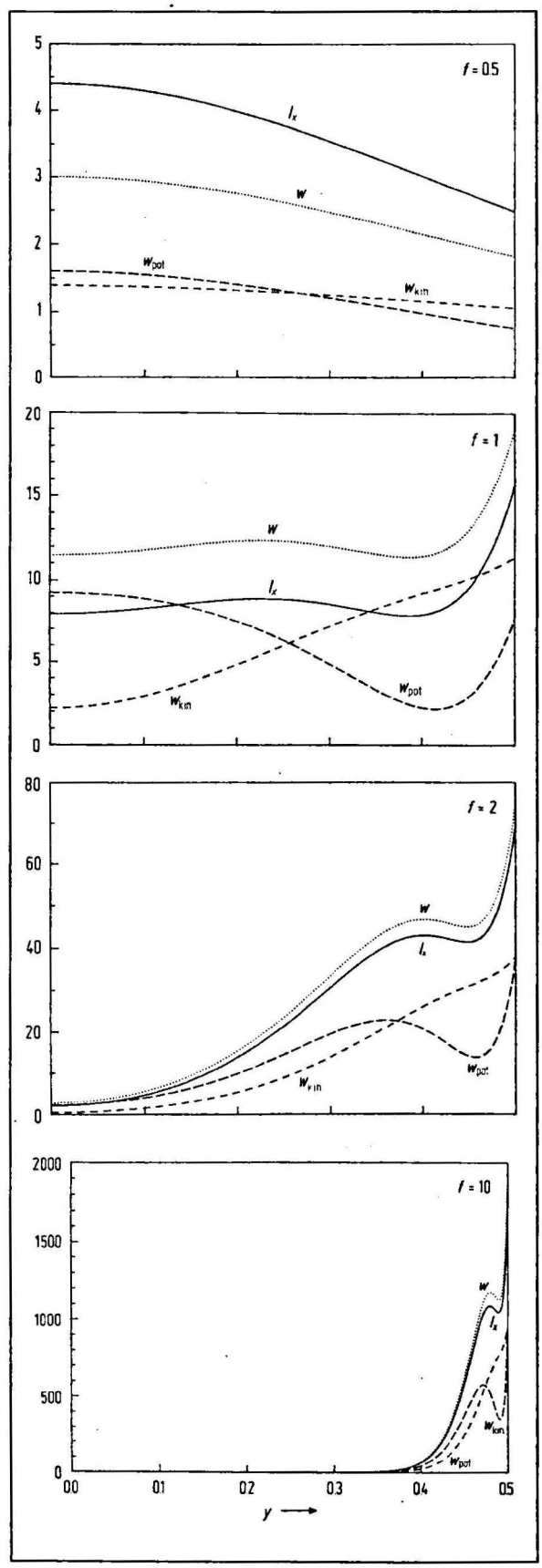

Fig. 7. Energy densities $w_{kin}(y) + w_{pot}(y) = w(y)$ and intensity component $I_x(y)$ of the quasi-longitudinal mode at various frequencies f ($\sigma = 0.3$).

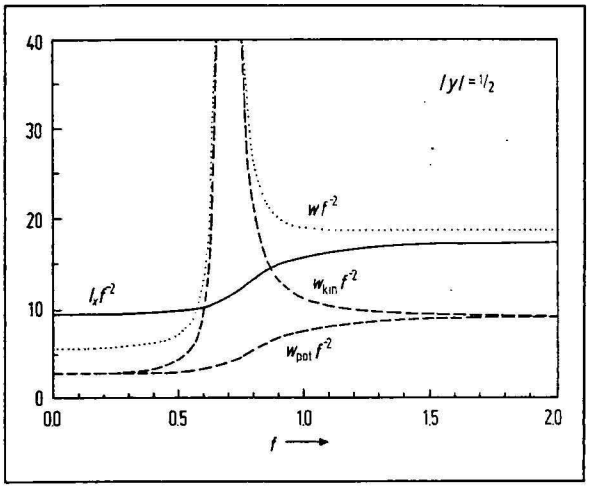

Fig. 8. Surface values of energy densities $w_{kin} + w_{pot} = w$ and intensity component I_x of the quasi-longitudinal mode divided by the frequency squared versus frequency ($\sigma = 0.3$).

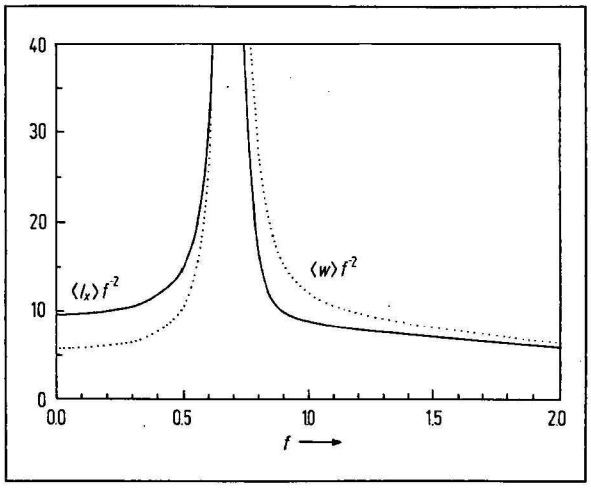

Fig. 9. Average energy density $\langle w \rangle$ and average intensity component $\langle I_x \rangle$ of the quasi-longitudinal mode divided by the frequency squared versus frequency ($\sigma = 0.3$).

Hence $\alpha_1 > 0$, $\alpha_2 = \mathrm{i}$, $k = \pi$ (wavelength = twice the thickness) and

$$\begin{aligned} u_x(y) &= -A\cos(\pi y), \\ u_y(y) &= \mathrm{i}A\sin(\pi y), \\ w_{kin}(y) &= \frac{\pi^2}{2}|A|^2\mu, \\ w_{pot}(y) &= \pi^2|A|^2\mu\cos^2(\pi y), \\ I_x(y) &= \sqrt{2}\pi^2|A|^2\mu\cos^2(\pi y), \\ \langle w_{kin}\rangle &= \langle w_{pot}\rangle = \frac{\pi^2}{2}|A|^2\mu, \\ \langle I_x\rangle &= \frac{\pi^2}{\sqrt{2}}|A|^2\mu. \end{aligned} \tag{44}$$

The requirement $u_x(\frac{1}{2}) = 1$ leads to an infinite amplitude and consequently to an infinite $w_{kin}(\frac{1}{2})$, while w_{pot} and I_x remain finite at the surface. It is striking that only the shear modulus μ is involved in (44) and indeed the strains and stresses,

$$\underline{\varepsilon} = \mathrm{i}\pi A\cos(\pi y)\begin{pmatrix} -1 & 0 \\ 0 & 1 \end{pmatrix}, \quad \underline{\sigma} = 2\mu\,\underline{\varepsilon}, \tag{45}$$

are pure shear! The singularity in Fig. 8 reflects the fact that the quasi-longitudinal mode at $f = \frac{1}{2}\sqrt{2}$ cannot be detected by strain gauges on the surface of the plate.

If one were particularly interested in the frequency region around $\frac{1}{2}\sqrt{2}$, one would rather choose $|u(\frac{1}{2})| = 1$ instead of (42). However, the rest of this section concentrates on the low- and high-frequency behaviour, where the description is more convenient with convention (42). (The measurement of surface intensity has been put forward by Pavić [20].)

At low frequencies the space-time averages $\langle w \rangle$ and $\langle I_x \rangle$ (Fig. 9) behave like the corresponding surface values, because there is little variation over the cross-section. At high frequencies the increase of the surface values with f^2 is accompanied by a confinement of the wave to an ever decreasing surface region resulting in an overall behaviour proportional to only the first power of the frequency. One finds for the low-frequency approximations

$$c = C = \sqrt{\frac{2}{1-\sigma}}, \tag{46}$$

$$\alpha_1 = \frac{\sigma}{1-\sigma}, \quad \alpha_2 = \mathrm{i}\sqrt{\frac{1+\sigma}{1-\sigma}}, \tag{47}$$

$$u_x = 1, \quad u_y = -\mathrm{i}\alpha_1 k y, \tag{48}$$

$$\langle w \rangle = 2w_{kin} = 2w_{pot} = 2\pi^2\mu f^2, \tag{49}$$

$$\langle I_x \rangle = \langle w \rangle C, \tag{50}$$

and for the high-frequency approximations (c_R = Rayleigh velocity; $\alpha_1 > \alpha_2 > 0$)

$$R_s = R_a = \mathrm{e}^{(\alpha_1-\alpha_2)k/2}, \tag{51}$$

$$\begin{aligned} u_x\left(\frac{1}{2}\right) &= \frac{\mathrm{i}}{2}A(1-\alpha_x)\mathrm{e}^{\alpha_1 k/2}, \\ u_y\left(\frac{1}{2}\right) &= \frac{\alpha_1}{2}A(1-\alpha_y)\mathrm{e}^{\alpha_1 k/2}, \end{aligned} \tag{52}$$

$$\begin{aligned} \langle w_{kin}\rangle = \tfrac{\pi}{8}\mu c_R f|A|^2\mathrm{e}^{\alpha_1 k} \\ \cdot\left\{\frac{1}{\alpha_1} + \alpha_1(1-4\alpha_y) + (\alpha_1\alpha_y)^2\left(\frac{1}{\alpha_2} + \alpha_2\right)\right\}, \end{aligned} \tag{53}$$

$$\langle I_x \rangle = 2\langle w_{kin}\rangle c_R. \tag{54}$$

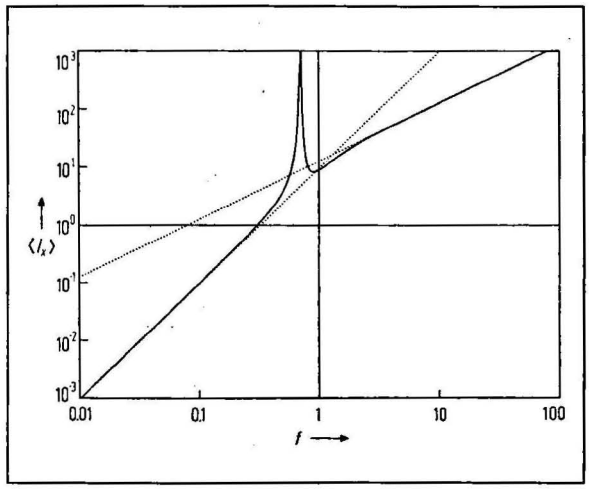

Fig. 10. Average intensity component $\langle I_x \rangle$ of the quasi-longitudinal mode with low- and high-frequency approximations (dotted lines) versus frequency ($\sigma = 0.3$).

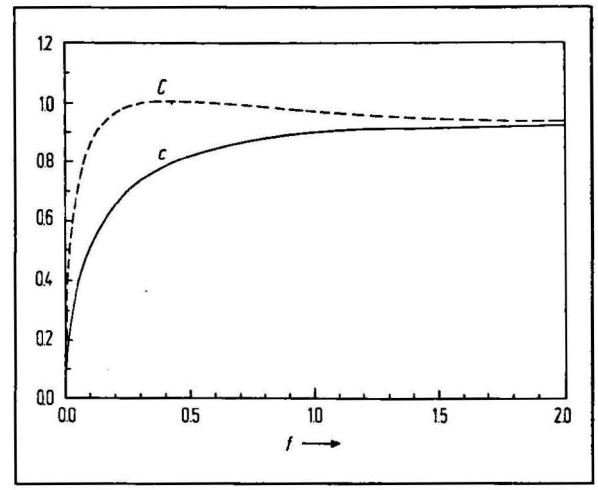

Fig. 11. Phase velocity c and group velocity C of the bending mode versus frequency ($\sigma = 0.3$).

At high frequencies the amplitude convention (42) leads to

$$|A|^2 = \frac{4\,e^{-\alpha_1 k}}{(1-\alpha_x)^2} \tag{55}$$

and thus to a linear frequency dependence of $\langle w \rangle$ and $\langle I_x \rangle$.

The ranges of applicability of these approximations to the average intensity may be inferred from Fig. 10. Apart from the region around the singularity the approximations look rather satisfactory. In fact, the errors are less than 20% for $f \leqq 0.4$ and $f \geqq 1.5$, respectively. The ranges with errors not exceeding 10% (1%) are $f \leqq 0.3$ (0.1) and $f \geqq 1.9$ (3.0).

5.2. The bending mode

Phase and group velocity of the fundamental antisymmetric mode are shown in Fig. 11. Its amplitude is chosen such that the displacement component normal to the surface is unity at the surface $y = 1/2$:

$$u_y(y = \tfrac{1}{2}) = 1\,. \tag{56}$$

The displacement field is plotted in Fig. 12 for various frequencies. The low frequency behaviour (constant u_y and small linear u_x) has a somewhat smaller frequency range of validity compared to the quasi-longitudinal wave. However, the transition to a surface wave appears to be "smoother" than in the case of the fundamental symmetric mode, because neither u_y nor u_x become zero at the surface. The transversal component u_y is always larger than the longitudinal component u_x.

The y-dependence of the various energy quantities at the four frequencies of Fig. 12 is shown in Fig. 13. At $f = 0.1$ energy density and intensity increase from the centre to the surface of the plate (Fig. 7, $f = 0.5$ shows the opposite behaviour!). As expected, with increasing frequency both fundamental modes exhibit more and more the same behaviour.

At high frequencies surface intensity and energy densities are proportional to the frequency squared (Fig. 14). For $f \to 0$ intensity and energy density behave differently because the group velocity of bending waves is proportional to $\sqrt{f}$. This is true both at the surface and on average (Fig. 15) since I_x and w are approximately constant over the cross-section.

At low frequencies one obtains to lowest order (simple bending wave theory):

$$c_B = \frac{\sqrt{2\pi f}}{\sqrt[4]{6(1-\sigma)}}, \quad C_B = 2c_B, \tag{57}$$

$$k_B = \sqrt[4]{6(1-\sigma)}\sqrt{2\pi f}, \tag{58}$$

$$u_x = -\mathrm{i}ky, \quad u_y = 1, \tag{59}$$

$$\langle w \rangle = 2w_{kin} = 2\pi^2 \mu f^2, \tag{60}$$

$$\langle I_x \rangle = \langle w \rangle C_B. \tag{61}$$

Evidently, the space-time average of the energy density is the same for both fundamental modes if the frequency approaches zero and the amplitudes obey (42) and (56), respectively. Note that $\langle w \rangle$ depends only on the shear modulus μ and not on the compressional modulus (which equals $(1+\sigma)/[3(1-\sigma)]$ in normalized form), whereas $\langle I_x \rangle$ depends like the group velocity C on both moduli. From (57) the average intensity of the bending mode is proportional to $f^{5/2}$.

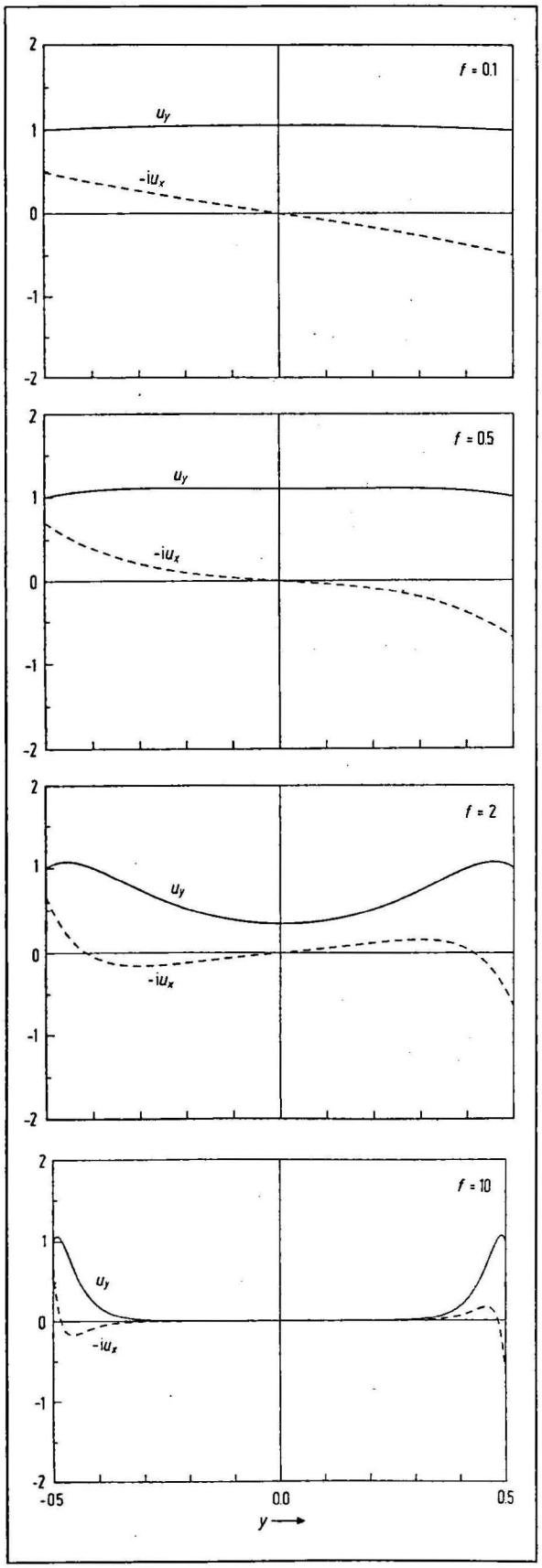

Fig. 12. Displacement components $u_x(y)$ and $u_y(y)$ of the bending mode at various frequencies $f(\sigma = 0.3)$.

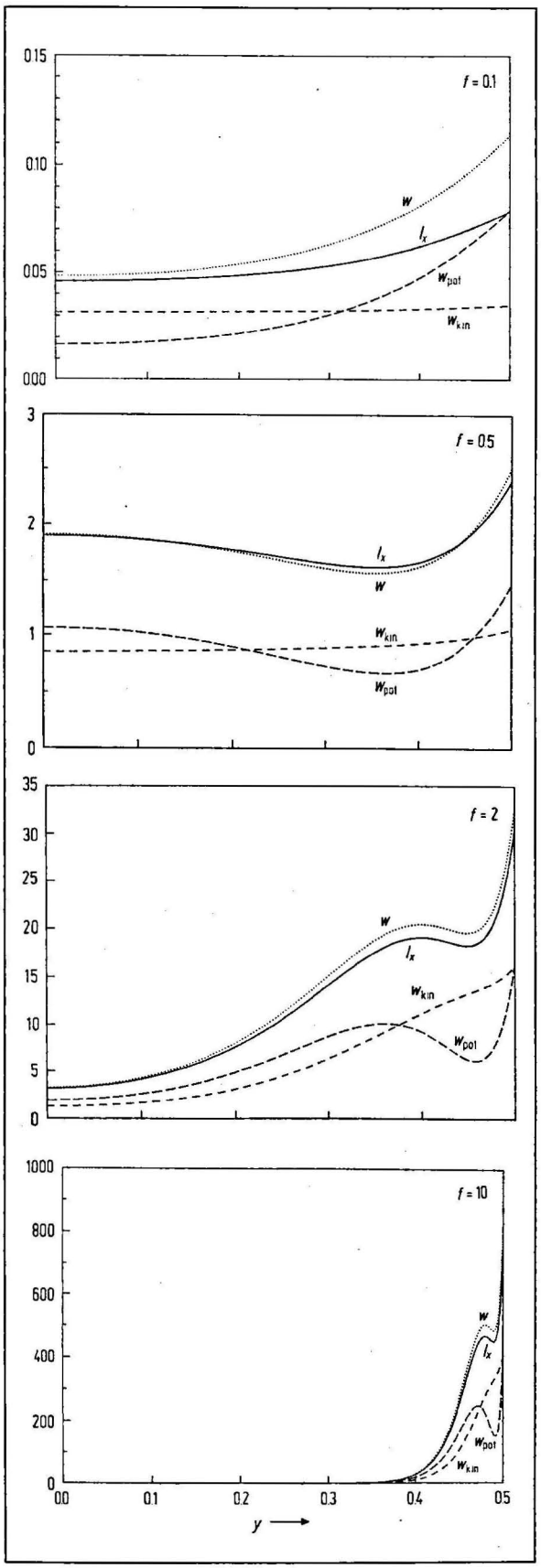

Fig. 13. Energy densities $w_{kin}(y) + w_{pot}(y) = w(y)$ and intensity component $I_x(y)$ of the bending mode at various frequencies $f(\sigma = 0.3)$.

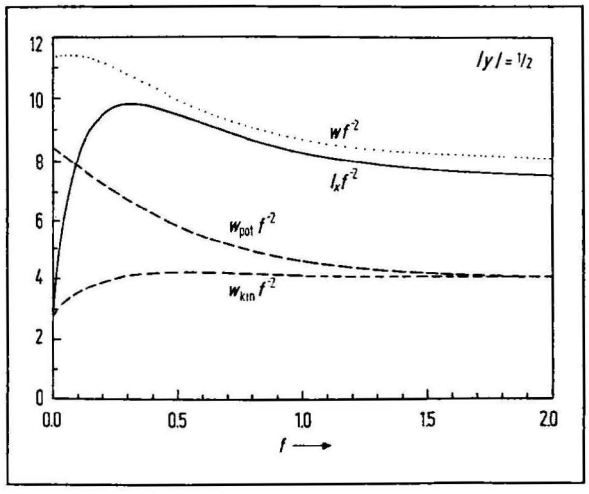

Fig. 14. Surface values of energy densities $w_{kin} + w_{pot} = w$ and intensity component I_x of the bending mode divided by the frequency squared versus frequency ($\sigma = 0.3$).

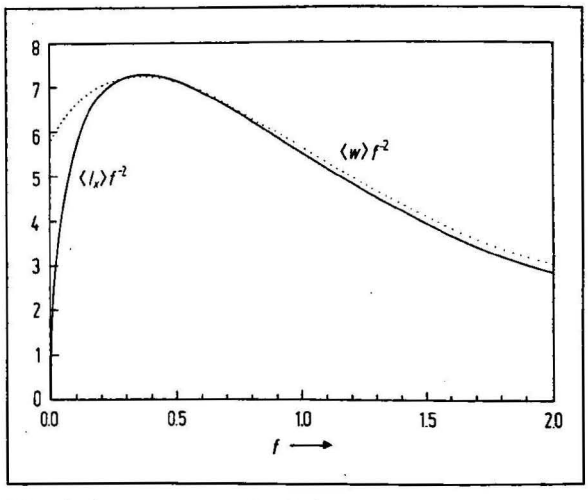

Fig. 15. Average energy density $\langle\omega\rangle$ and average intensity component $\langle I_x\rangle$ of the bending mode divided by the frequency squared versus frequency ($\sigma = 0.3$).

The expressions for the high-frequency approximation are identical with eqs. (51 to 54). The results, however, are different for both fundamental modes because the amplitudes have been chosen differently. From (56) we obtain

$$|A|^2 = \frac{4\,\mathrm{e}^{-\alpha_1 k}}{\alpha_1^2 (1-\alpha_y)^2}. \tag{62}$$

The log-log-plot Fig. 16 gives an impression of the accuracy of the low- and high-frequency approximations. The gaps within which the approximations cannot be used are wider than in the quasi-longitudinal case, especially if only small errors are allowed. The errors are less than 20% for $f \leqq 0.13$ and $f \geqq 0.67$. The ranges with errors not exceeding 10% (1%) are $f \leqq 0.065$ (0.007) and $f \geq 0.77$ (3.0).

5.3. Conventional bending wave intensity

The bending wave intensity is usually measured by means of two accelerometers mounted to the surface of the plate along the propagation direction x. Their mutual distance should be small compared to the bending wavelength in order to obtain a good estimate for the spatial derivative of the acceleration, which is needed in the familiar formula for the bending wave intensity I_B,

$$I_B = -\frac{\sqrt{B\varrho h}}{\omega h}\,\mathrm{Re}\left\{a_y \int \frac{\partial a_y^*}{\partial x}\,\mathrm{d}t\right\}, \tag{63}$$

where $B = E h^3/[12(1-\sigma^2)]$ is the bending stiffness and a_y is the normal component of the acceleration at the surface $y = 1/2$. (Usually the bending wave intensity is defined as $h I_B$, which has the dimension power per unit length. We prefer definition (63), which is consistent with the more general intensity definition (14).) Eq. (63) is valid for sinusoidal waves and can be evaluated to

$$I_B = \frac{h}{2}\sqrt{\frac{E\varrho}{3(1-\sigma^2)}}\,\omega^2 k\,|u_y(y=\tfrac{1}{2})|^2 \tag{64}$$

with

$$|u_y(y=\tfrac{1}{2})|^2 = |A|^2 \alpha_1^2 (1-\alpha_y)^2 \cosh^2(\alpha_1 k h/2), \tag{65}$$

which reduces to

$$I_B = \frac{1-2\sigma}{2\sqrt{6(1-\sigma)^3}}\,\omega^2 k \tag{66}$$

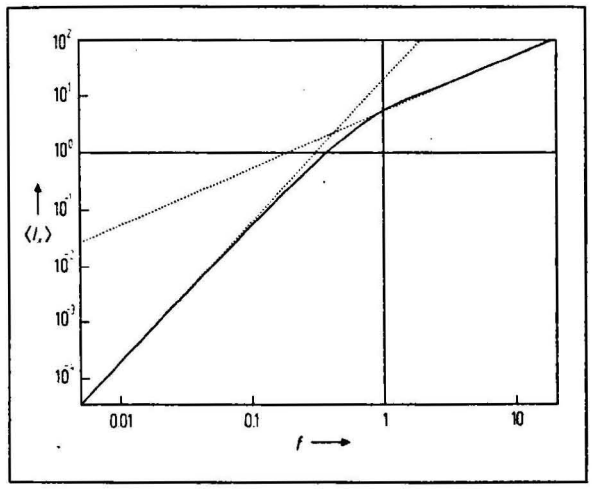

Fig. 16. Average intensity component $\langle I_x\rangle$ of the bending mode with low- and high-frequency approximations (dotted lines) versus frequency ($\sigma = 0.3$).

after adopting the amplitude convention (56) and normalizing according to section 3. If one substitutes k by ω/c with the low frequency approximation (57), one recovers the result (61). Since the ratio between I_B and $\langle I_x \rangle$ according to (61) is equal to $c_B/c \geqq 1$ and since $\langle I_x \rangle$ according to (61) overestimates the exact $\langle I_x \rangle$ (see Fig. 16), the approximation I_B systematically overestimates the intensity. The error relative to the exact $\langle I_x \rangle$,

$$\delta = \frac{I_B - \langle I_x \rangle}{\langle I_x \rangle}, \tag{67}$$

is proportional to the frequency for $f \to 0$ and amounts to a few percent even at $f = 0.01$ (Fig. 17). The upper limits for an error not exceeding 20%, 10%, 1% are $f \leqq 0.073$, 0.037, 0.004, respectively ($\sigma = 0.3$).

Simple bending wave theory is considered to be valid if the wavelength is greater than six times the thickness of the plate, i.e. for $k < \pi/3 \approx 1.05$, which corresponds to frequencies below $f = 0.073$ ($\sigma = 0.3$). Beyond this frequency region the error of the velocity approximation (57) exceeds 10% [19] and the error of the intensity approximation (66) exceeds 20%. In many applications errors of this size may be readily acceptable. If a higher accuracy is desired or necessary, the error of the conventional bending wave intensity measurement can now be corrected on the basis of eq. (67). The error may either be estimated from Fig. 17 or calculated from eqs. (40) and (66). Thus the intensity of the bending mode can in principle be measured at arbitrary frequencies with the conventional technique. It appears to be practically feasible at least below the onset of higher modes, i.e. below $f = 0.5$, where only the possible excitation of the quasi-longitudinal mode may complicate matters. (The contribution of the quasi-longitudinal mode to the y-component of the acceleration can be eliminated by measuring on both surfaces of the plate, because the displacement fields of the two fundamental modes possess different symmetry.)

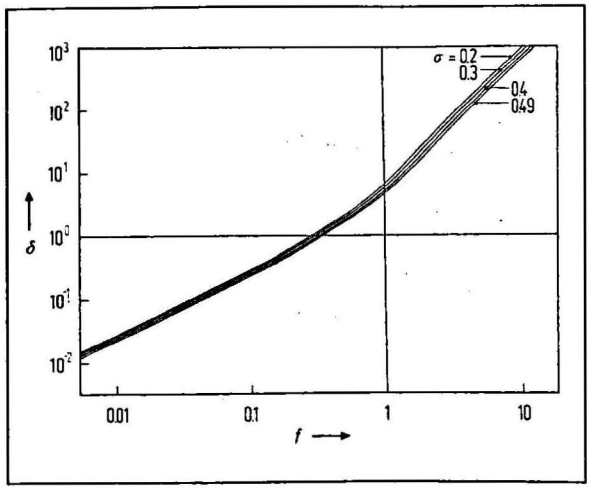

Fig. 17. Relative error of the bending wave intensity (66) versus frequency for various values of Poisson's ratio. δ is defined in (67).

6. Conclusion

Exact and explicit expressions have been worked out for the intensity and the time-averaged energy densities of an arbitrary propagating mode in a homogeneous and elastically isotropic plate of constant thickness. The spatial averages of these quantities across the thickness of the plate have also been obtained analytically. The only prerequisite for the application of these expressions to a particular mode is the knowledge of its phase and group velocity. Of course, in general these velocities must be calculated numerically.

Particular attention has been paid to the quasi-longitudinal mode and the bending mode. Low- and high-frequency approximations have been derived and their ranges of applicability have been studied. Finally, the accuracy of the conventional technique of measuring the intensity of bending waves has been assessed. A correction factor has been determined which allows an extension of this technique to higher frequencies provided one is able to isolate the bending mode portion of the measured acceleration.

Exploration of intensity and energy density of higher non-pure-shear modes is straightforward and does not require more effort than in the case of the two fundamental modes once the velocities are known.

Appendix

This appendix addresses briefly the question of how to determine phase and group velocities of the two fundamental non-pure-shear modes. Low-frequency expansions of the phase velocities are available (see e.g. [21]), and it is well-known that in the high-frequency limit phase and group velocity approach the velocity c_R of Rayleigh surface waves, which is a solution of the (normalized) cubic equation for c_R^2:

$$c_R^6 - 8\,c_R^4 + 8(3-2\mu)\,c_R^2 - 16(1-\mu) = 0. \tag{A1}$$

Mindlin [22] has developed an approximation c_M for the phase velocity of the bending mode, which can be used with relatively little error for arbitrary frequencies:

$$\left[\frac{1}{c_R^2} - \frac{3}{(\pi f)^2}\right] c_M^4 - \left[1 + \frac{2}{c_R^2(1-\sigma)}\right] c_M^2 + \frac{2}{1-\sigma} = 0. \tag{A2}$$

The corresponding group velocity C_M can also be obtained explicitly via the general relation

$$C = \frac{c}{1 - \frac{f}{c}\frac{\mathrm{d}c}{\mathrm{d}f}}. \tag{A3}$$

The three-digit accuracy claimed by Mindlin for c_M could not be confirmed, however. The difference to the exact phase velocity may even affect the second decimal digit (Fig. A1) and the approximation C_M may even be worse.

In view of these deficiencies Mindlin's approximation has been taken only as a starting point for a numerically exact solution of the dispersion relation (9). (The Van Wijngarden-Dekker-Brent Method [23] is used for root finding.) Except for very low frequencies, where $C = 2c$ holds, the group velocity of the bending mode has been determined by (A3) with numerical differentiation of c with respect to f. (It appears possible to arrive at an explicit expression for $\mathrm{d}c/\mathrm{d}f$ by means of an implicit differentiation of the dispersion relation (9). The numerical differentiation could then be avoided.)

There are no serious problems with an accurate computation of the bending mode velocities; α_1 and α_2 and hence the whole dispersion relation remain real for arbitrary frequency. The case of the quasi-longitudinal mode is more complicated. While α_1 stays real for any frequency, α_2 is imaginary for low frequencies and real for frequencies where the phase velocity becomes smaller than unity. Further, $\alpha_2 = \mathrm{i}$ at $f = \frac{1}{2}\sqrt{2}$ leads to a singularity in the dispersion relation due to $(1 + \alpha_2^2)^2 = 0$ and $\tanh(\alpha_2 k/2) = \infty$. In order to obtain solution in the vicinity of $f = \frac{1}{2}\sqrt{2}$ one has to deal with

$$\frac{\cosh(\alpha_2 k/2)}{(1+\alpha_2^2)^2} = \frac{\cos(\pi|\alpha_2| f/c)}{(1+\alpha_2^2)^2} \tag{A4}$$

at

$$f = \tfrac{1}{2}\sqrt{2}(1+p), \quad c = \sqrt{2}(1+q) \tag{A5}$$

with small values of p and q. The numerator of (A4) is expanded around $\pi/2$,

$$\cos\left(\frac{\pi}{2} + s\right) = -s\left(1 - \frac{s^2}{3!} + \frac{s^4}{5!} \mp \ldots\right) \tag{A6}$$

with

$$s = \frac{\pi}{2}\left(\frac{1+p}{1+q}\sqrt{1+4q+2q^2} - 1\right), \tag{A7}$$

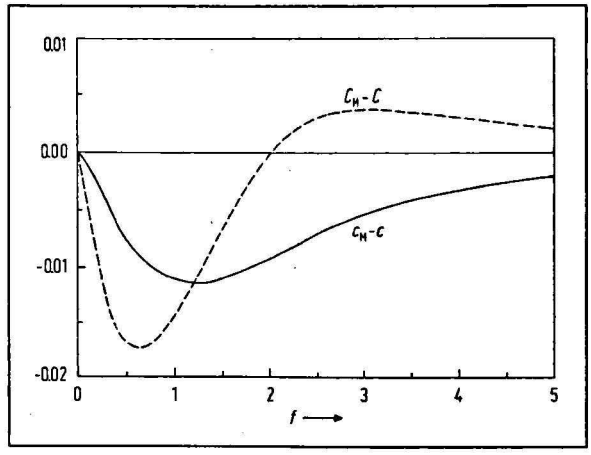

Fig. A1. Absolute error of Mindlin's approximations c_M and C_M to the exact phase and group velocities c and C versus frequency ($\sigma = 0.3$).

while the denominator becomes

$$(1+\alpha_2^2)^2 = 4q^2(2+q)^2. \tag{A8}$$

One can show that $p = -q$ in the limit $q \to 0$. During the iteration procedure, however, p and q are considered as independent variables. Therefore we write

$$p = -q - Hq^2 \tag{A9}$$

and determine H from

$$H = -\frac{p+q}{q^2}. \tag{A10}$$

This looks bad for $q \to 0$, but with reasonable starting values for the root finding procedure eq. (A10) did not cause any trouble. This is related to the fact that H becomes independent of p and q for the solution q at frequencies with $p \to 0$. (The case $p = 0$ should be treated separately, of course.) (A7) can now be rewritten as

$$s = \frac{\pi}{2(1+q)}[(1 - q - Hq^2)\sqrt{1+4q+2q^2} - 1 - q)]$$

$$= \frac{\pi}{2(1+q)}K. \tag{A11}$$

Since s will be divided by q^2, bracket K should be determined quite accurately. We do this by an iterative solution of

$$\tilde{K} = \frac{-(2H+6) - 6Hq + (H^2+4H+2)q^2 + 4H(1+H)q^3 + 2H^2q^4}{\tilde{K}q^2 + 2(1+q)} \tag{A12}$$

starting with $\tilde{K} = 0$ on the right-hand side ($K = \tilde{K}q^2$). Thus one arrives at

$$\frac{\cosh(\alpha_2 k/2)}{(1+\alpha_2^2)^2} = \frac{-\pi\tilde{K}}{8(1+q)(2+q)^2}\left(1 - \frac{s^2}{3!} + \frac{s^4}{5!} \mp \ldots\right) \tag{A13}$$

in a numerically convenient manner. Apart from the truncation of the series (A 6) no approximations have been made. Therefore (A 13) can be applied in an appreciable range around $f = \frac{1}{2}\sqrt{2}$ provided α_2 remains imaginary, i.e. $c > 1$.

The frequency f_1, where the phase velocity of the quasi-longitudinal mode is equal to one, obeys the transcendental equation

$$\frac{\pi}{4}\sqrt{2(1-\sigma)}\, f_1 = \tanh\left(\frac{\pi f_1}{\sqrt{2(1-\sigma)}}\right) \qquad \text{(A 14)}$$

and is shown in Fig. A 2 as a function of Poisson's ratio σ. (Negative values of σ appear not to have been discussed so far for plate waves, although this range is not generally forbidden within the framework of linearized elastodynamics, which only requires positive moduli for shear and compression, i.e. $-1 < \sigma < 1/2$. Nevertheless it would be worthwhile to investigate the dispersion diagram for $\sigma < 0$. For instance, the solutions $c = \sqrt{2}$ at $f = \frac{1}{2}\sqrt{2}$ (independent of σ) and $c = 1$ at $f_1 = \frac{1}{2}\sqrt{2}$ for some negative σ ($\sigma \approx -0.27$) indicate that the two velocity values belong to different modes, whereas for $\sigma > 0$ they belong to the same mode!) The region around f_1 can be treated by expanding $\sinh(\alpha_2 k/2)$ and by subsequent cancellation of α_2, which removes the singularity of the dispersion relation at $\alpha_2 = 0$.

A more detailed discussion of the numerical solution of the Rayleigh-Lamb frequency equations, especially for higher modes, is certainly beyond the scope of the present paper. For some reason no descriptions of numerical procedures appear to exist in the literature. Perhaps, considerations like this appendix have been regarded as trivial in the past. Nowadays, the development and publication of a reliable and efficient computer code for the velocities of plate waves is overdue.

Note added in proof: Negative values of Poisson's ratio have now been discussed extensively by A. Freedman (J. Sound Vib. **137** [1990], 209–266).

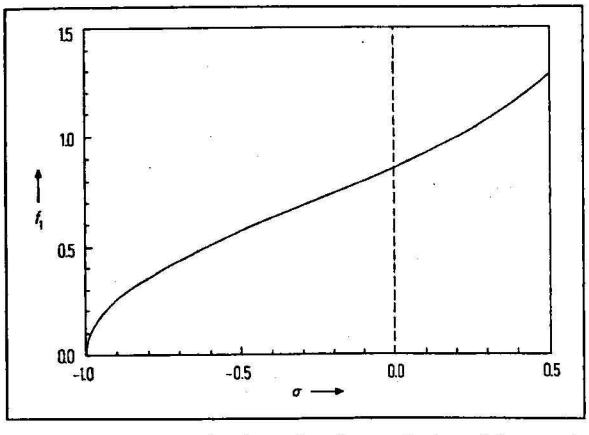

Fig. A 2. Frequency f_1 where the phase velocity of the quasi-longitudinal mode equals one versus Poisson's ratio.

References

[1] Noiseux, D. U., Measurement of power flow in uniform beams and plates. J. Acoust. Soc. Amer. **47** [1970], 238–247.

[2] Pavić, G., Measurement of structure-borne wave intensity, Part I: Formulation of the methods. J. Sound Vib. **49** [1976], 221–230.

[3] Verheij, J. W., Cross spectral density methods for measuring structure-borne power flow on beams and pipes. J. Sound Vib. **70** [1980], 133–139.

[4] Rasmussen, P. and Rasmussen, G., Intensity measurements in structures. Proc. 11th ICA Paris 1983, Vol. 6, pp. 231–234.

[5] Quinlan, D., Measurement of power flow and other energy quantities within plates. Proc. Internoise Munich 1985, pp. 1259–1262.

[6] Kruppa, P., Measurement of structural intensity in building constructions. Appl. Acoustics **19** [1986], 61–74.

[7] Meyer, B. and Bouyaakoub, N., Intensimétrie vibratoire dans les barres. Rev. d'Acoust. **82** [1987], 121–125.

[8] Linjama, J. and Lahti, T., Experiments of structural intensity measurement using the one-transducer frequency response method. Proc. Internoise Avignon 1988, Vol. 1, pp. 595–598.

[9] Carniel, X., Limitations théoriques et expérimentales sur la mesure accélérométrique de l'intensité vibratoire dans les poutres. J. Acoust. **1** [1988], 189–195.

[10] Maysenhölder, W. and Schneider, W., Sound bridge localization in buildings by structure-borne sound intensity measurements. Acustica **68** [1989], 258–262.

[11] Achenbach, J. D., Wave propagation in elastic solids. North Holland, Amsterdam 1984, p. 209.

[12] Tuan, H.-S., On bulk waves excited at a groove by Rayleigh waves. J. Appl. Phys. **46** [1975], 36–41; eq. (24).

[13] Biryukov, S. V., Rayleigh-wave scattering by two-dimensional surface corrugations in oblique incidence. Sov. Phys. Acoust. **26** [1980], 272–276; eq. (12).

[14] Seshadri, S. R., Energy transport velocity of surface elastic waves. J. Appl. Phys. **54** [1983], 1699–1703; eq. (49).

[15] Tamm, K. und Weis, O., Untersuchungen über periodische Wellen, exponentielle und komplexe Nahfelder im begrenzten Festkörper. Acustica **9** [1959], 275–288.

[16] Meeker, T. R. and Meitzler, A. H., Guided wave propagation in elongated cylinders and plates. In: Physical Acoustics (edited by W. P. Mason) Vol. 1 A, Academic Press, New York 1964, pp. 111–167.

[17] Maysenhölder, W., to be published in J. Acoust. Soc. Am.

[18] Biot, M. A., General theorems on the equivalence of group velocity and energy transport. Phys. Rev. **105** [1957], 1129–1137.

[19] Cremer, L. and Heckl, M., Structure-borne sound (translated and revised by E. E. Ungar). Springer, Berlin 1988.

[20] Pavić, G., Structural surface intensity: An alternative approach in vibration analysis and diagnosis. J. Sound Vib. **115** [1987], 405–422.

[21] Maysenhölder, W., Some didactical and some practical remarks on free plate waves. J. Sound Vib. **118** [1987], 531–538.

[22] Mindlin, R. D., Influence of rotatory inertia and shear on flexural motions of isotropic, elastic plates. J. Appl. Mech. **18** [1951], 31–38.

[23] Press, W. H., Flannery, B. P., Teukolsky, S. A., Vetterling, W. T., Numerical recipes: The art of scientific computing. Cambridge University Press 1986, pp. 251.